AFRL-OSR-VA-TR-2014-0359

Fundamental Materials Studies for Advanced High Power Microwave and Terahertz

John Booske
UNIVERSITY OF WISCONSIN SYSTEM MADISON WI

12/10/2014
Final Report

Air Force Research Laboratory
AF Office Of Scientific Research (AFOSR)/ RTB
Arlington, Virginia 22203
Air Force Materiel Command

REPORT DOCUMENTATION PAGE

Form Approved
OMB No. 0704-0188

PLEASE DO NOT RETURN YOUR FORM TO THE ABOVE ORGANIZATION.

1. REPORT DATE *(DD-MM-YYYY)*	2. REPORT TYPE	3. DATES COVERED *(From - To)*
06-12-2014	Final Technical Performance Report	October 1, 2011 - September 30, 2014

4. TITLE AND SUBTITLE
Fundamental Materials Studies for Advanced High Power Microwave and Terahertz Vacuum Electronic Radiation Sources

5a. CONTRACT NUMBER

5b. GRANT NUMBER
FA9550-11-1-0299

5c. PROGRAM ELEMENT NUMBER

6. AUTHOR(S)
Booske, John H.

5d. PROJECT NUMBER

5e. TASK NUMBER

5f. WORK UNIT NUMBER

7. PERFORMING ORGANIZATION NAME(S) AND ADDRESS(ES)
University of Wisconsin-Madison
Research & Sponsored Programs
21 N Park St STE 6401
Madison WI 53715-1218; 608-262-0252

8. PERFORMING ORGANIZATION REPORT NUMBER

9. SPONSORING/MONITORING AGENCY NAME(S) AND ADDRESS(ES)
Air Force Office of Scientific Research
875 N Randolph St Room 3112
Arlington, VA 22203

10. SPONSOR/MONITOR'S ACRONYM(S)
AFOSR

11. SPONSOR/MONITOR'S REPORT NUMBER(S)

12. DISTRIBUTION/AVAILABILITY STATEMENT

13. SUPPLEMENTARY NOTES

14. ABSTRACT

The results of research sponsored by this grant address two fundamental questions relevant to the advancement of THz-regime device technology (0.1 - 3 THz). First, they establish a detailed, comprehensive fundamental understanding, of THz-regime conductivity, including the effects of materials imperfections (impurities, defects, surface roughness) in conductive materials (including metals, semiconductors, and graphene). This includes providing accurate predictive theoretical models, robustly validated by experimental measurements. Second, they establish a fundamental understanding of low-emission-barrier scandate cathodes and identify related, alternative cathode materials systems for advanced vacuum electronic cathodes for high power THz-regime sources.

15. SUBJECT TERMS

16. SECURITY CLASSIFICATION OF:			17. LIMITATION OF ABSTRACT	18. NUMBER OF PAGES	19a. NAME OF RESPONSIBLE PERSON
a. REPORT	b. ABSTRACT	c. THIS PAGE			John H Booske
			UU		19b. TELEPHONE NUMBER *(Include area code)* 608-262-8548

Abstract

The results of research sponsored by this grant address two fundamental questions relevant to the advancement of THz-regime device technology (0.1 - 3 THz). First, they establish a detailed, comprehensive fundamental understanding, of THz-regime conductivity, including the effects of materials imperfections (impurities, defects, surface roughness) in conductive materials (including metals, semiconductors, and graphene). This includes providing accurate predictive theoretical models, robustly validated by experimental measurements. Second, they establish a fundamental understanding of low-emission-barrier scandate cathodes and identify related, alternative cathode materials systems for advanced vacuum electronic cathodes for high power THz-regime sources.

Summary of research results

The original objectives of this research grant were:

- to establish a fundamental understanding of the terahertz-regime (0.1 – 3 THz) *effective conductivity* of conductive materials, incorporating realistic non-idealities, and
- to establish a fundamental understanding of *low-emission-barrier scandate cathodes* and explore related, alternative cathode materials systems.

Both objectives were met and exceeded beyond our original expectations. Key accomplishments included:

1. We successfully fabricated high purity copper film samples with large (~ 1 μm) grains and controlled (varied) surface roughness (15-75 nm). Using these samples **we solved the challenge of determining a quantitatively-accurate predictive model for THz-regime conductivity including the effects of surface roughness.** The details of this work have been submitted for publication [3] and are also published in Matt Kirley's Ph.D. dissertation, pending approval by his defense committee in December 2014.
    a. With high purity (low impurity atom concentration) and grain sizes much larger than electron scattering mean free path, we were able to isolate the effect of surface roughness on the THz-regime conductivity of copper, separating surface-roughness scattering from impurity or grain-boundary scattering on ohmic dissipation.
    b. We successfully measured the DC and THz-regime conductivity of copper film samples at 400, 650, and 850 GHz with varied surface roughness.
    c. We successfully compared the measured results with predictions of numerous theoretical models and were able to conclude that combining measurements of DC conductivity, AFM measurements of surface roughness, and application of the Hammerstad-Bekkadal model for high-frequency conductivity including surface-roughness [1] provides a reliable, quantitatively-accurate predictive model for THz-regime conductivity.

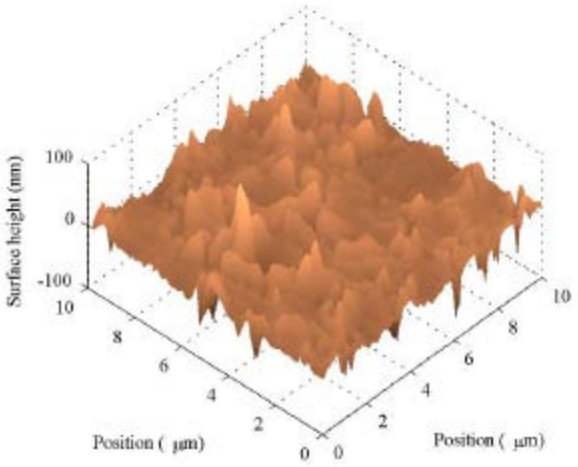

Fig. 1. Projection of AFM measurement of a copper sample after roughening by acid etch.

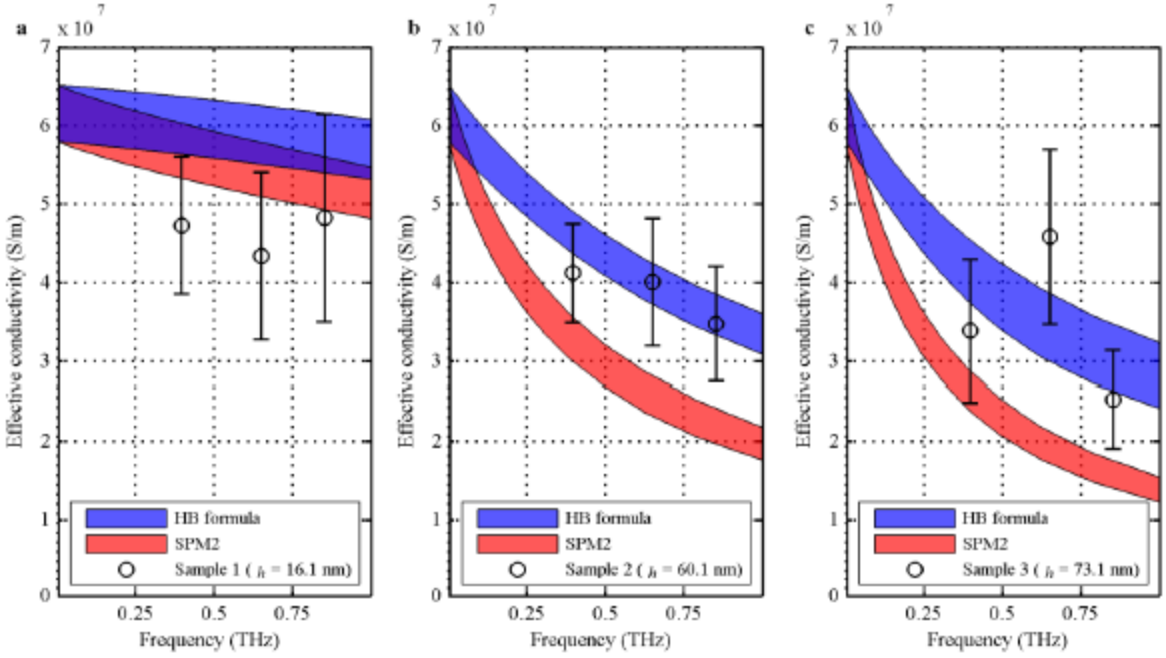

Fig. 2. THz conductivity measurements and predictions for copper surfaces with rms roughness height equal to a) 16.1 nm, b) 60.1 nm, and c) 73.1 nm. The data confirm that the Hammerstad-Bekkedal (HB) model is a reliable predictor of the conductivity including the effects of surface roughness. They also show that a more sophisticated, second-order-perturbation-theory (SPM2) model is a less accurate predictor of the conductivity. This means that future design of THz-regime metallized components can be done reliably, without need for *guestimating* the surface conductivity of the surfaces.

2. We successfully fabricated highly-doped (n = 6 × 10^{19} cm^{-3}) silicon samples and measured their THz-regime conductivity (0.4 – 0.85 GHz). This research demonstrated and explained the difference between THz-regime conductivity of moderately-doped Si and highly-doped Si. We are drafting a manuscript of this work for publication and it is also summarized in an appendix of Matt Kirley's PhD dissertation, pending approval by his defense committee in December 2014.
    a. Our prior measurements of moderately-doped Si ((n = 10^{12}-10^{14} cm^{-3}) (supported with a prior grant) demonstrated that conventional Drude theory does *not* suffice to accurately predict THz-regime conductivity [2]. In contrast, under *this* grant **we**

have determined that conventional Drude theory *does* suffice as a reliable, quantitative predictor of THz conductivity for highly-doped Si.

b. We have been able to explain these discrepancies. At moderate doping densities ($n < 10^{17}$), the quasi-static assumption of conventional Drude theory, i.e., that $\omega\tau << 1$, does not hold. Furthermore, at moderate and low doping densities, carriers are scattered mainly by electron-phonon interactions and the conventional Drude theory's assumption of a single relaxation time, τ, is not representative of the distribution of scattering times experienced by charge carriers. At high doping density, however, ($n > 10^{17}$ cm^{-3}), the scattering is much more frequent, such that $\omega\tau << 1$. Furthermore, at high doping density, all interactions become increasingly electrostatically screened while a greater number of ionized impurities are present for scattering electrons. Thus, scattering, dominated by Coulomb collisions, is weakly dependent on electron energy so that a single value of τ is a better approximation to the true τ distribution than in the moderate and low-doping case.

3. We **developed a self-consistent multiphysics tool for examining the carrier dynamics of two-dimensional electron systems and applied it to calculating the THz conductivity of graphene supported on a substrate.** The details of this computational tool were published in [4] and part of Chapter 3 in Nishant Sule's PhD dissertation.
   a. The multiphysics computational tool comprises ensemble Monte Carlo (EMC), a semi-classical technique used to numerically solve the Boltzmann transport equation in order to simulate carrier motion, coupled with finite-difference time-domain (FDTD) and molecular dynamics (MD). FDTD method, used for solving the Maxwell's curl equations and MD, used for calculating the inter-particle electrostatic force, are used for coupling electrodynamics with the carrier motion in a self-consistent manner.
   b. The EMC/FDTD/MD method is extended for simulating carrier dynamics in supported graphene systems with charged impurities present near the interface of graphene and the substrate.

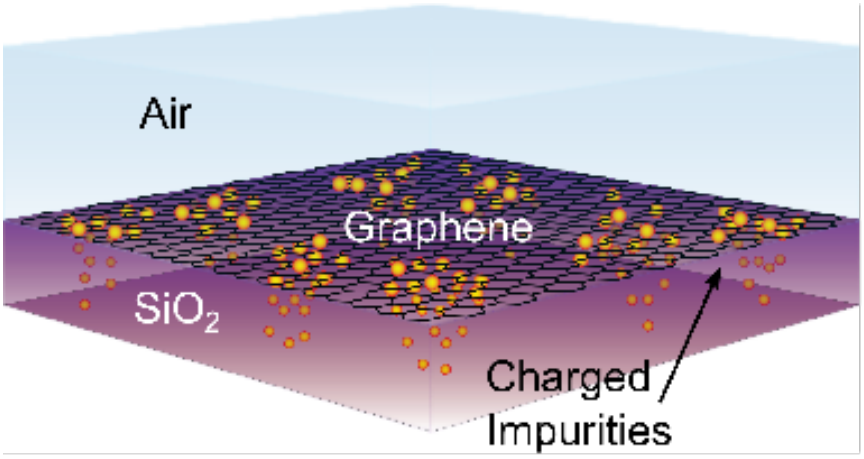

Fig. 3. Schematic of the simulated structure: single-layer graphene rests on an SiO_2 substrate, with charged impurities present near the interface between the two. Carrier transport is simulated by including both electrons and holes in the graphene layer, while the positively charged ions near the interface and within the SiO_2 substrate remain stationary.

4. We examined the effect of charged impurity distributions on carrier transport in graphene on SiO_2 using the EMC/FDTD/MD method. The results of this work were published in [5] and are contained in Chapter 4 of the PhD dissertation of N. Sule.
    a. **We showed that clustered impurities of characteristic width 40-50 nm generate 20-nm-sized electron-hole puddles similar to experimental observations.** Moreover, **clustered impurities play an important role in the carrier dynamics of supported graphene.**
    b. **The carrier density dependent THz conductivity *σ(n)* calculated using clustered impurity distributions reproduced the important features observed in experimental measurements.** For example: The residual conductivity and the linear-region slope of the conductivity versus carrier density dependence are determined by the impurity distribution and the measured slope can be used to estimate the impurity density in experiment. Furthermore, the high-density sublinearity in the conductivity stems from carrier-carrier interactions.

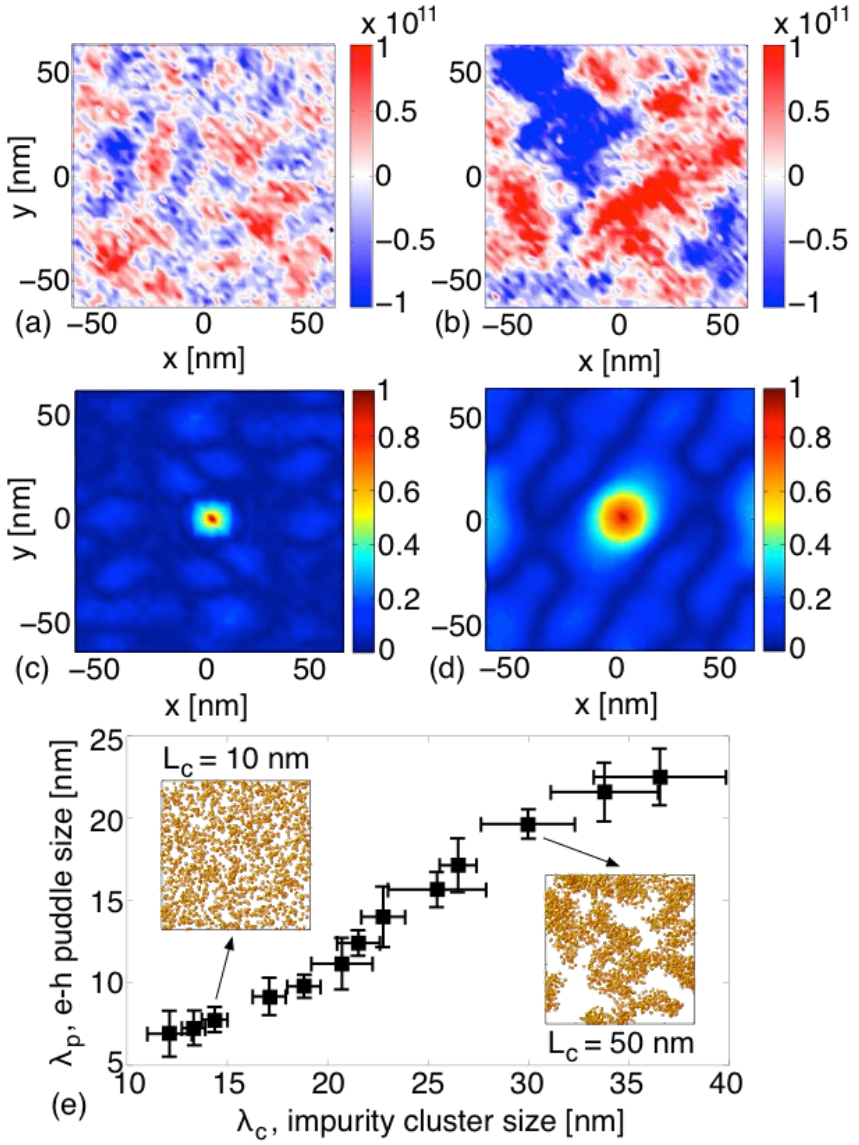

Fig. 4. Carrier density distribution (blue, electrons; red, holes) depicting the electron-hole puddles formed in graphene at the Dirac point for (a) uniform random (λ_c = 22 nm) and (b) clustered (λ_c = 46 nm) impurity distributions, both with impurity sheet density equal to 5×10^{11} cm^{-2}. The average size of the electron-hole puddles, λ_p, is estimated from the FWHM (yellow ring) of the normalized carrier density spatial autocorrelation function, shown in (c) and (d), corresponding to the random and clustered impurity distributions from (a) and (b), respectively. The estimated puddle size from (c) is λ_p = 6 nm and that from (d) is λ_p = 20 nm. (e) Characteristic electron-hole puddle size λ_p as a function of the average impurity cluster size λ_c. Each data point corresponds to a single value of the clustering parameter L_c (swept from 0 to 60 nm in the increments of 5 nm) and is the average of 14 simulation runs; the error bars denote the standard deviations. Insets: Illustrative impurity distributions, nearly random on the left (L_c = 10 nm) and highly clustered on the right (L_c = 50 nm).

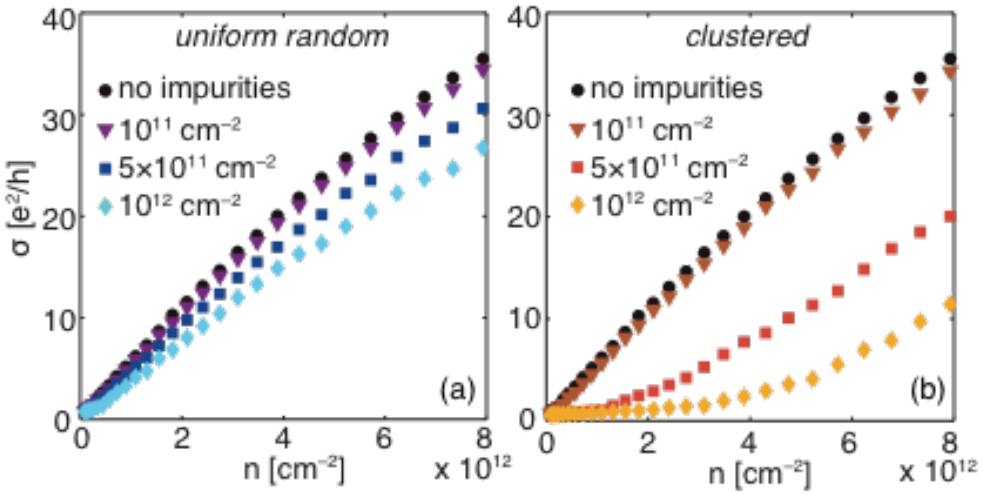

Fig. 5. Conductivity of graphene on SiO_2 for (a) uniform random (L_c = 0, λ_c = 22 nm) and (b) clustered (L_c = 50 nm, λ_c = 46 nm) impurity distributions, at impurity sheet densities of 10^{11} cm^{-2} (triangles), 5×10^{11} cm^{-2} (squares), 10^{12} cm^{-2} (diamonds), and without impurities (circles).

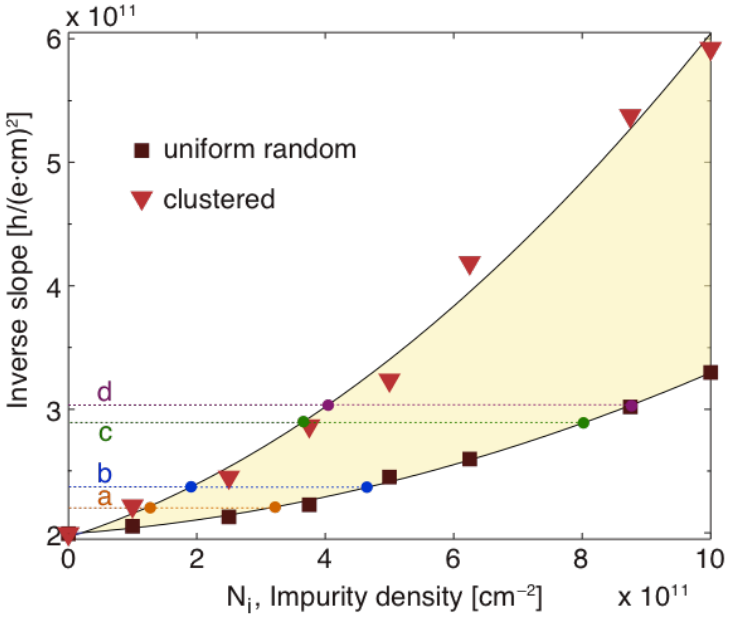

Fig. 6. Inverse slope of $\sigma(n)$ as a function of the sheet impurity density for graphene on SiO_2 at room temperature. Squares denote the uniform random impurity distribution (L_c = 0, λ_c = 22 nm), while triangles correspond to clustered impurity distributions that would give realistic electron-hole puddle sizes (L_c = 50 nm, λ_c = 46 nm). The horizontal lines a–d correspond to the inverse slope values obtained in several experiments: line a, L. Vicarelli et al., *Nat. Mater.* **11**, 865 (2012); line b, F. Schedin et al., *Nat. Mater.* **6**, 652 (2007); line c, Novoselov et al., *PNAS* **102**, 10451 (2005); and line d, Novoselov et al., *Science* **306**, 666 (2004). The impurity density range between the intercepts of an inverse-slope horizontal line with the clustered and random distribution curves (i.e., the range within the lightly shaded area) yields an estimate of the impurity density range.

5. We examined the room-temperature complex conductivity σ(ω) of suspended and supported graphene at terahertz frequencies (100 GHz–10 THz) for a wide range of electron (n = 10^{12}–10^{13} cm^{-2}) and impurity densities (N_i = 8×10^{10}–2×10^{12} cm^{-2}) by

employing the EMC/FDTD/MD method. The results of this work were published in [6] and are contained in Chapter 5 of the PhD dissertation of Nishant Sule.

a. **We obtain excellent agreement between our calculation with clustered impurities and the experimentally measured σ(ω),** while the σ(ω) for a uniform random distribution of impurities does not yield good agreement for any reasonable impurity density. Thus, providing more **evidence to the important role of clustered impurity distributions on carrier transport in supported graphene.**
b. We show that the choice of the substrate (SiO2 or h-BN), which is relevant for modifying the conductivity with substrate-engineering is important only at frequencies below 4 THz and when $N_i/n < 0.1$. Electron-impurity interactions dominate for $N_i/n > 0.1$, and transport enters the electron-hole puddle regime for $N_i/n > 0.5$.
c. We find that **the simple Drude model,** with an effective scattering rate Γ and Drude weight D as parameters, **fits the calculated *σ(ω)* for supported graphene very well, owing to electron-impurity scattering.** Γ decreases with increasing n faster than $n^{-1/2}$ and is insensitive to electron-electron interaction. Both electron-electron and electron-impurity interactions reduce the Drude weight D, and its dependence on n is sublinear.

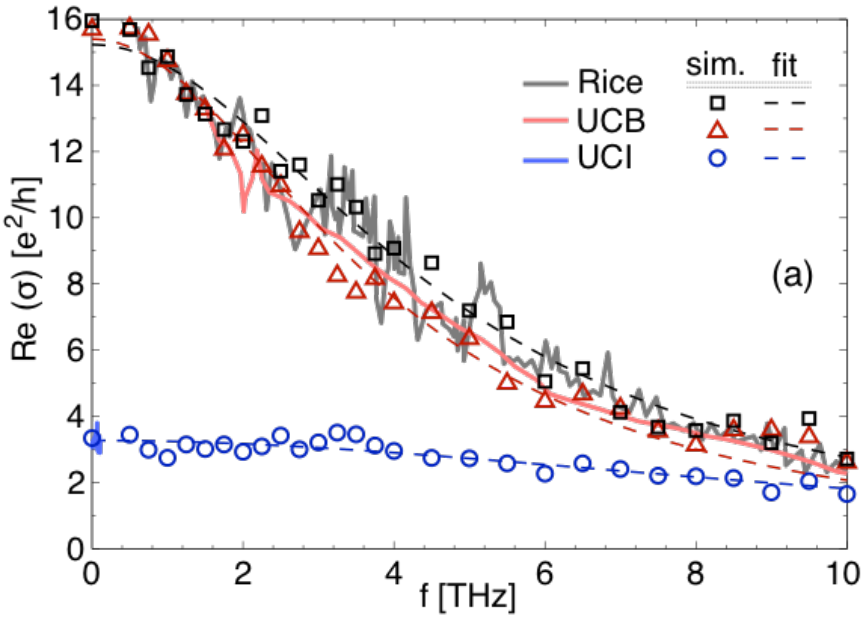

Fig. 7.. Real part of *σ(ω)* as a function of frequency. Calculated values based on the EMC/FDTD/MD simulation (squares, triangles, and circles) match, respectively, the experimental data from N. Rouhi et al., *Nano Res.* **5**, 667 (2012) (blue: UC Irvine), L. Ju et al., *Nat. Nanotechnol.* **6**, 630 (2012) (red: UC Berkeley), and L. Ren et al., *Nano Lett.* **12**, 3711 (2012) (black: Rice University). Dashed lines are Drude-model fits to the simulation data.

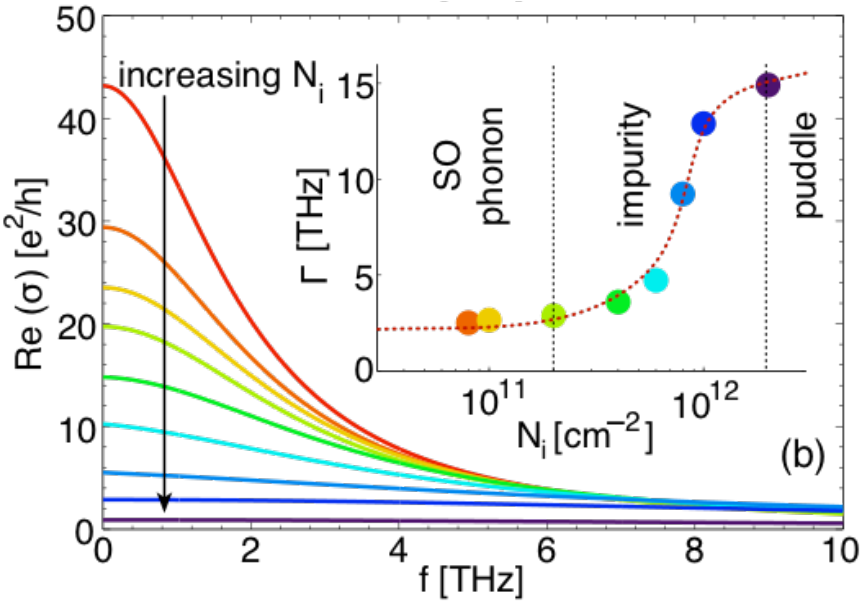

Fig. 8. Generalized-Drude-model best fits to the calculated $\sigma(\omega)$ for graphene on SiO_2 with different impurity densities, from top (red) to bottom (purple): $N_i = 0$, 8×10^{10}, 10^{11}, 2×10^{11}, 4×10^{11}, 6×10^{11}, 8×10^{11}, 10^{12}, and 2×10^{12} cm^{-2}. Inset: Γ corresponding to the generalized-Drude-model fits in the main panel as a function of N_i. Circle colors in the inset correspond to the curve colors in the main panel.

6. Using Density Functional Theory (DFT) **we have successfully explained the mechanism by which scandium oxide Sc_2O_3, (or scandate) cathodes achieve superior cathode emitter properties.** While alternative theories have been ventured, our explanation is the simplest, is consistent with familiar surface dipole and impurity doping mechanisms for lowering work functions, and explains how Sc_2O_3 conducts current at high temperatures sufficiently well to function as a copious thermionic emitter of electrons with good long-life stability (due to low volatility of the Sc_2O_3) . These results have been published in [7] and [8].
    a. The principal results of [7] include
        i. Density Functional Theory (DFT) used to investigate intrinsic defect formation as a mechanism by which bulk Sc_2O_3 (an insulator) could act as a good conductor in the thermionic cathode environment (T ~ 1200 K, P ~ 10^{-10} Torr) to obtain a better understanding of observed enhanced emission from scandate thermionic devices.
        ii. From calculating the formation energies of relevant intrinsic defects in the bulk Sc_2O_3 structure, and further by developing a defect model whereby the defect, electron and hole concentrations were calculated by maintaining a self-consistent value of the Fermi energy, it is expected that Sc_2O_3 will behave natively as a p-type semiconductor under cathode operating conditions.
        iii. By using a simple Ohm's law argument, it was found that to maintain the experimentally observed emission current densities of approximately 10 A/cm^2 through a 200 nm Sc_2O_3 film, the Sc_2O_3 must have a conductivity of 10^{-4} $\Omega^{-1}cm^{-1}$ or higher to avoid dielectric breakdown. A very small

impurity concentration (order of 1 part per billion) is necessary to realize this minimum conductivity value because intrinsic defects alone do not produce a sufficient number of free carriers, and these impurities are expected to be present in all experimental Sc_2O_3 samples.

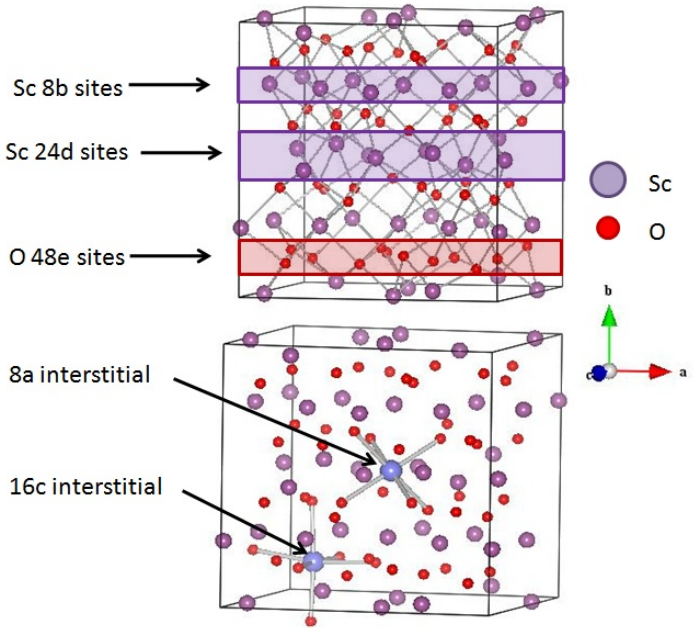

Fig. 9. Sc_2O_3 cubic bixbyite conventional unit cell depicting native and interstitial Wyckoff positions used in this study.

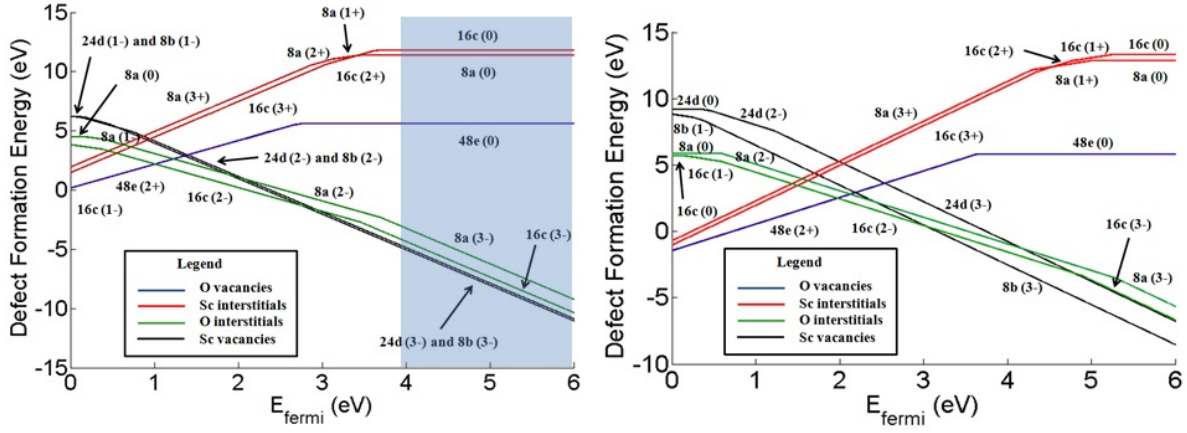

Fig. 10. Calculated defect formation energies for intrinsic defects in Sc_2O_3 as a function of Fermi level for (left) GGA and (right) HSE functionals. Intermediate values of $\mu_{Sc}^{Sc_2O_3}$ and $\mu_{O}^{Sc_2O_3}$ (cathode operating conditions: T= 1200 K and P = 10^{-10} Torr) were used in both cases. The shaded portion indicates Fermi energies that lie above the calculated GGA bandgap.

b. The principal results of [8] include:

i. DFT was used to calculate the surface energy barrier (work function) and thermodynamic stability of varying coverages of atomic Ba and Ba-O dimer adsorption on the (011) and (111) Sc_2O_3 surface terminations to investigate the role Ba plays in lowering the work function of Sc_2O_3 in thermionic cathodes.

ii. It was found that for bare Sc_2O_3 surface terminations, the order of stability (from most to least stable) is: (111) > (011) > (001). Additionally, it was found that atomic Ba adsorption was unstable for all surface coverages and terminations considered. However, partial monolayer coverages of Ba-O on Sc_2O_3 (011) were found to be stable relative to the chosen reference state of BaO. These stability calculations indicate that real devices containing Sc_2O_3 will contain mainly (111) and (011)-oriented surface facets, and Ba will preferentially adsorb on the (011) terminations as a sub-monolayer of BaO.

iii. The lowest calculated surface energy barriers for electron removal when atomic Ba is present were 2.12 and 2.04 eV for the (011) and (111) surfaces, respectively. The lowest surface energy barrier for Ba-O coverage was 1.21 eV on Sc_2O_3 (011) for a partial monolayer. This surface configuration provides a plausible and straightforward explanation of observed enhanced emission in scandate thermionic devices.

iv. The mechanism of surface barrier lowering was found to consist of a surface dipole component as well as an electron (n-type) doping component. It was found that combined n-type doping and surface dipole modification yielding a surface barrier lowering that was less than the two contributions would yield separately.

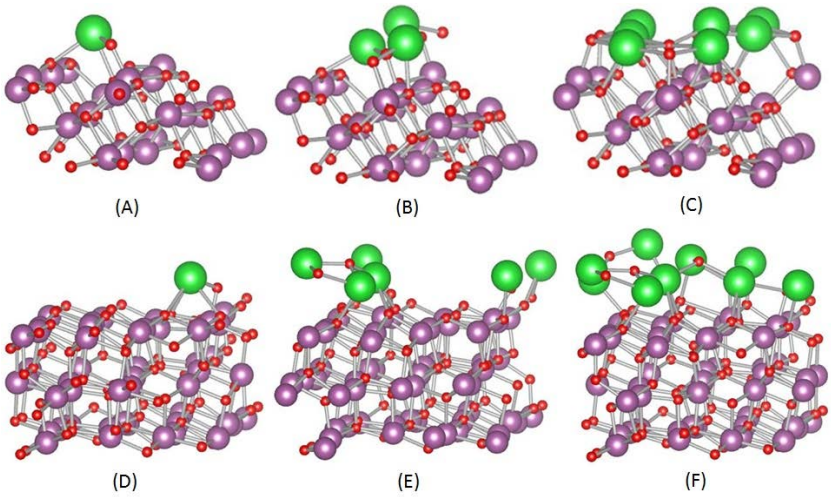

Fig. 11. Sc_2O_3 (011) and (111) slabs depicting fully relaxed Ba-O dimer geometries for several example coverages. (A), (B) and (C) are coverages of 1, 3, and 7 Ba-O per (011) surface unit cell. (D), (E) and (F) are coverages of 1, 6 and 9 Ba-O per (111) surface unit cell. A stable chain geometry of O-Ba-O bonds forms at coverages between 3-6 Ba-O.

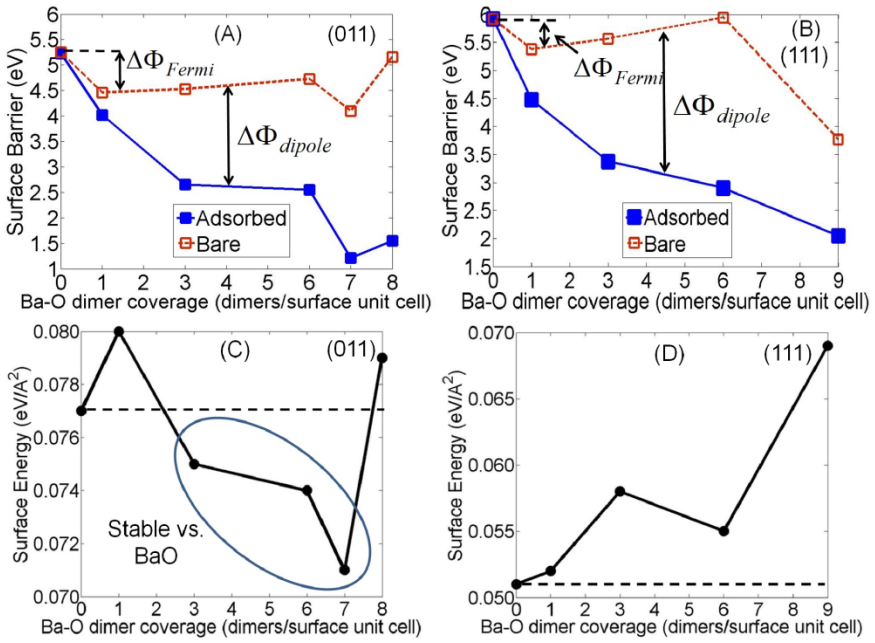

Fig. 12. Surface barrier as a function of Ba-O coverage for the (011) termination (A) and (111) termination (B). Solid blue lines are surface barriers of the Ba-O-terminated surface while dashed red lines are the surface barriers of the opposing bare surfaces. Surface energy as a function of Ba-O coverage for the (011) termination (C) and (111) termination (D) are plotted. The dashed lines in (C) and (D) mark the surface energy of the bare reference slabs for comparison. Stable dimer coverages (relative to BaO) on (011) are circled, characterized by surface energies which are lower than the bare reference (011) surface energy.

7. Using Density Functional Theory (DFT) we have successfully **identified a brand-new class of materials based upon the perovskite structure** that have potential to provide superior high power microwave (vacuum electronic) device cathodes (thermionic or field emission). **This is the first instance of identifying an advanced, superior cathode material candidate using *ab initio*, quantitative computational modeling.** Future research using high-throughput screening of various perovskite alloys has the potential to identify candidate compounds that would provide lower work function, longer lifetime cathodes without the need for volatile impregnates such as barium. Our results under this grant have made such high-throughput computational screening possible by identifying a bulk alloy property that is an approximate reliable predictor of low work function. This bulk property is much faster to calculate than surface properties such as work function. **There are many important benefits that could be realized from such work, including low-cost, long-lifetime HPM devices, and longer lifetime for critical defense technologies such as high power radar and ECM transmitters and vacuum electronic (traveling wave tube) satellite power amplifiers.** A manuscript of these results is being drafted for publication. The principal results include:
    a. DFT was used to calculate the (001)-oriented AO and BO_2-terminated work functions of eighteen different technologically relevant 3*d* transition metal perovskites: the $LaBO_3$ series (B = Sc, Ti, V, Cr, Mn, Fe, Co, Ni), $SrBO_3$ series (B = Ti, V, Fe, Co), $La_{1-x}Sr_xMnO_3$ (x= 0.0625, 0.125, 0.25, and 0.375) (LSM),

$LaAlO_3$ and $Ba_{0.5}Sr_{0.5}Co_{0.75}Fe_{0.25}O_3$ (BSCF). The purpose of investigating these materials was threefold: to ascertain the range of work function values these materials can exhibit; to understand the physics of what governs the work function of perovskite materials, and to find a new, low work function material for application in high power devices and thermionic energy conversion.

b. The work function range of these materials is broad and varies from as low as 1.79 eV for AO-terminated $SrVO_3$ to 6.87 eV for BO_2-terminated $LaAlO_3$. $SrVO_3$ is the lowest work function material examined here, and presents itself as a promising candidate to replace existing thermionic cathode materials given its low work function, metallic conductivity, and stable (001) surface terminations. Additionally, it was found that doping $SrVO_3$ with Ba may result in a Ba-rich surface that could exhibit a work function as low as 1.07 eV.

c. We utilized the O 2*p* band center calculated from the electronic density of states of the bulk materials as an electronic structure descriptor to develop an understanding of what governs the work function physics, and found there is semi-quantitative linear correlation between both the AO and BO_2 work functions and the value of the O 2*p* band center of the corresponding bulk materials. This relationship may be used in future work of high-throughput computational screening of the O 2*p* band centers of many bulk perovskite materials to survey a larger composition space for stable materials that are expected to fall within an expected work function range, e.g. searching for other low work function materials.

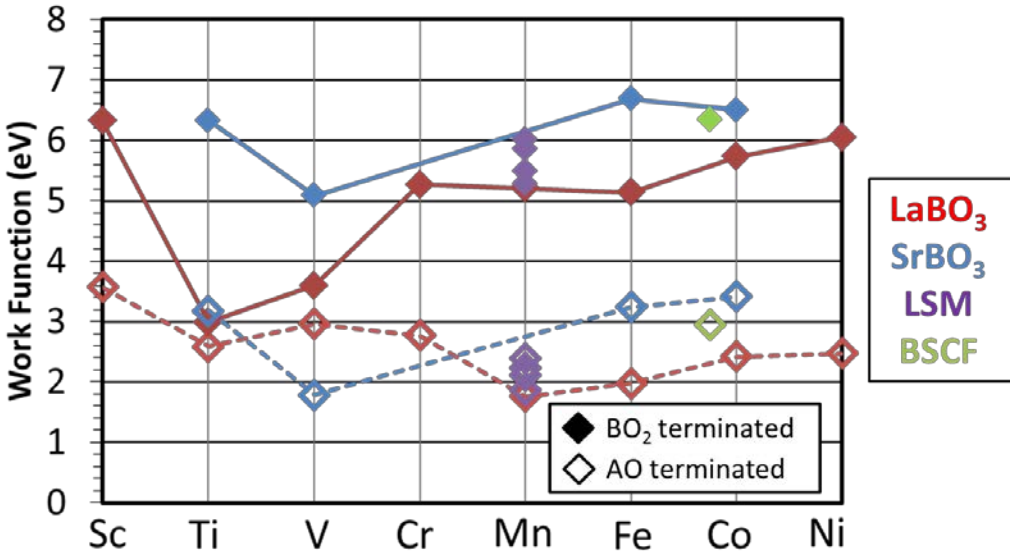

Fig. 13. Trend of (001) AO and BO_2 terminated surface work functions for the 18 perovskite materials as a function of B-site element across the periodic table. The solid (open) symbols connected with a solid (dashed) line are the BO_2 (AO) work functions, respectively. Red, blue, purple, and green symbols signify the $LaBO_3$, $SrBO_3$, LSM, and BSCF series of materials, respectively. $LaAlO_3$ is not shown on the plot but has calculated work functions of 3.25 eV and 6.87 eV for the AO and BO_2 terminated surfaces, respectively.

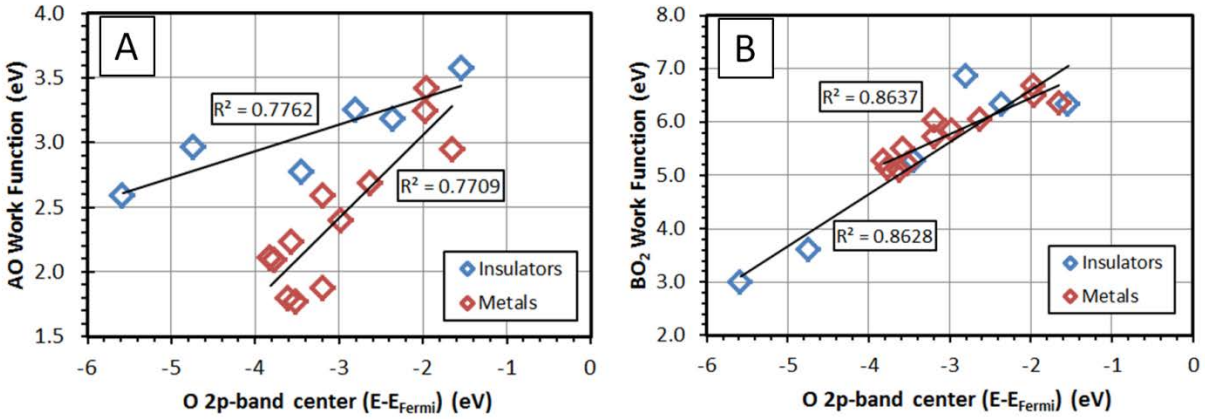

Fig. 14. Plots of calculated work functions for the AO (A) and BO_2-terminated surfaces (B) of ABO_3 materials as a function of the O 2*p* band center of bulk ABO_3 materials. In both plots, the blue symbols represent insulating perovskites while the red symbols represent metallic perovskites. In (A) there is a semi-quantitative linear correlation for AO work function versus bulk O 2*p* band center. In (B) there is also a linear correlation of BO_2 work function with the bulk O 2*p* band center.

References cited of work *not* resulting from this grant

[1] E. Hammerstad and O. Jensen, "Accurate Models for Microstrip Computer-Aided Design," in *Microwave Symposium Digest, 1980 IEEE MTT-S International*, 1980, p. 407.

[2] B.B. Yang, S.L. Katz, K.J. Willis, M.J. Weber, I. Knezevic, S.C. Hagness, and J.H. Booske, "A High-Q Terahertz Resonator for the Measurement of Electronic Properties of Conductors and Low-Loss Dielectrics," *IEEE Trans. Terahertz Sci. Technol.*, vol. 2, no. 4, pp. 449-459, July 2012.

References of work resulting from this grant

[3] M.P. Kirley and J.H. Booske, "Terahertz conductivity of copper surfaces," *IEEE Trans. Terahertz Sci. and Technol.* (submitted, 2014).

[4] N. Sule, K.J. Willis, S.C. Hagness, I. Knezevic, "EMC/FDTD/MD simulation of carrier transport and electrodynamics in two-dimensinoal electron systems," *J. Comput. Electron.* **12**, 563-571 (2013).

[5] N. Sule, S.C. Hagness, I. Knezevic, "Clustered impurities and carrier transport in supported graphene," *Phys. Rev. B* **89**, 165402 (2014)

[6] N. Sule, K.J. Willis, S.C. Hagness, "Terahertz-frequency electronic transport in graphene," *Phys. Rev. B* **90**, 045431 (2014)

[7] R.M. Jacobs, J.H. Booske, D. Morgan, "Intrinsic defects and conduction characteristics of Sc_2O_3 in thermionic cathode systems", *Phys. Rev. B.*, 2012, 86, 054106.

[8] R.M. Jacobs, J.H. Booske, D. Morgan, "Electron emission energy barriers and stability of Sc_2O_3 with Adsorbed Ba and Ba-O", *J. Phys. Chem. C*, 2014, 118 (34), 19742–19758.

Additional conference papers and presentations supported by this work

[9] "Study of the Effect of Nanofabricated Surface Roughness on Conductivity in the Terahertz Regime with a High-Q Resonator," Benjamin Yang, Matthew Kirley, John Booske, 36th Int'l Conf. Infrared, Millimeter and Terahertz Waves, paper M2C.3 (Houston, TX, Oct 2-7, 2011).

[10] "Analysis of Atmospheric Attenuation due to Water Content at 400 and 650 GHz," Marcus Weber; Benjamin Yang; Mark Kulie; Ralf Bennartz; John Booske, 36th Int'l Conf. Infrared, Millimeter and Terahertz Waves, paper M3B.3 (Houston, TX, Oct 2-7, 2011).

[11] "Fabrication and Test of Terahertz Extended Interaction Klystrons," Richard Dobbs, Mark Hyttinen, Brian Steer, Khanh Nguyen, Edward Wright, David Chernin, Jeffrey Calame, Baruch Levush, Scott Barker, John Booske, Monica Blank, Frank Maiwald, 36th Int'l Conf. Infrared, Millimeter and Terahertz Waves, paper Tu3B.2 (Houston, TX, Oct 2-7, 2011).

[12] "Measurements of Near Terahertz Conductivity of Doped Silicon using a High Quality Factor Resonant Cavity," Matthew Kirley; Benjamin Yang; Keely Willis; Marcus Weber; Nishant Sule; Susan Hagness; Irena Knezevic; John Booske, 36th Int'l Conf. Infrared, Millimeter and Terahertz Waves, paper W5.20 (Houston, TX, Oct 2-7, 2011).

[13] "Effect of Surface Roughness on Metallic Conductivity in the Terahertz Regime," M. Kirley, B.B. Yang, J.H. Booske, 53rd Annual Mtg American Phys. Soc. Div. Plasma Physics, paper T07.3 (Salt Lake City, Utah, (Nov. 14-18, 2011).

[14] "*Ab initio* Model of Intrinsic Defects in Sc_2O_3 for Thermionic Cathode Systems ," Ryan Jacobs, Dane Morgan, and John Booske, 13th IEEE International Vacuum Electronics Conference and 9th International Vacuum Electron Sources Conference (co-located), Monterey, CA (April 24-26, 2012).

[15] "Study of the Effect of Surface Roughness and Skin Depth on the Conductivity of Metals at 650 GHz," Matt Kirley and John H. Booske, 13th IEEE International Vacuum Electronics Conference and 9th International Vacuum Electron Sources Conference (co-located), Monterey, CA (April 24-26, 2012).

[16] "Electromagnetic Attenuation due to Water Vapor Measured at 400 GHz," Marcus J. Weber, Benjamin B. Yang, Matt Kirley, Mark S. Kulie, Ralf Bennartz, and John H.

Booske, 13th IEEE International Vacuum Electronics Conference and 9th International Vacuum Electron Sources Conference (co-located), Monterey, CA (April 24-26, 2012).

[17] "Terahertz conductivity of rough metallic surfaces," M.P. Kirley, N. Carlsson, B.B. Yang, J.H. Booske, abstract 3P-44, IEEE International Conference on Plasma Science, Edinburgh, UK (July 8-12, 2012).

[18] "Reduced conductivity of nanorough surfaces at 650 GHz," M. P. Kirley, N. Carlsson, Benjamin B. Yang, and J. H. Booske, 54th Annual Meeting of the APS Division of Plasma Physics, Providence, RI, (October 29-November 2, 2012).

[19] "AFOSR-funded research at University of Wisconsin-Madison," John. Booske, Susan Hagness, Irena Knezevic, Dane Morgan, John Scharer, Nils Carlsson, David Holmgren, Ryan Jacobs, Sarah Katz, Matt Kirley, Brian Kupczyk, Marcus Weber, Xun Xiang, Ben Yang, AFOSR Workshop, San Antonio, Texas, January 16, 2012.

[20] "Measurement of the Intrinsic Conductivity of Copper at Near-THz Frequencies," M.P. Kirley and J.H. Booske, 2013 USNC-URSI National Radio Science Meeting (Boulder, CO, Jan 9-12, 2013).

[21] "Surface resistance of copper from 400 to 850 GHz," M.P. Kirley and J.H. Booske, 14th IEEE Int'l Conference on Vacuum Electronics (IVEC) (Paris, France, May 21-23, 2013). **Selected as finalist for Best Student Paper Award.**

[22] "Emission energy barriers of scandate surfaces with adsorbed Ba and Ba-O using Density Functional Theory," R.M. Jacobs, D. Morgan, J.H. Booske, 14th IEEE Int'l Conference on Vacuum Electronics (IVEC) (Paris, France, May 21-23, 2013).

[23] "Increased surface resistance of rough copper surfaces in the terahertz regime," M.P. Kirley and J.H. Booske, IEEE Pulsed Power and Plasma Science (PPPS) Conference, (San Francisco, CA, June 16-21, 2013).

[24] "Reduced Conductivity of Copper Between 400 and 850 GHz," M.P. Kirley and J.H. Booske, 55th Annual Meeting of the American Physical Society Division of Plasma Physics (Denver, CO, November 11-15, 2013).

[25] "Reflectivity of Rough Copper Surfaces at Submillimeter Frequencies," M.P. Kirley and J.H. Booske, USNC-URSI Radio Science Meeting (Boulder, CO, Jan. 8-11, 2014).

[26] "Perovskite oxides: New candidate materials for low work function electron emitters," Ryan Jacobs, Dane Morgan, John H. Booske, IEEE International Vacuum Electronics Conference, (Monterey, CA, April 22-24, 2014).

[27] "Increased Resistance of Rough Copper Surfaces at Terahertz Frequencies," M. P. Kirley and John. H. Booske, IEEE International Vacuum Electronics Conference, (Monterey, CA, April 22-24, 2014). **Selected as finalist for Best Student Paper Award.**

[28] “Work function physics of 3d transition metal perovskites using Density Functional Theory,” R.M Jacobs, J. Booske, and D. Morgan, Materials Science & Technology Conference, (Pittsburgh, PA, October 12-16, 2014).

[29] Sule N., Willis, K. J., Hagness S. C., and Knezevic I., "Multiphysics simulations of carrier transport and electrodynamics in two-dimensional electron systems," General Assembly and Scientific Symposium (URSI-GASS), 2014 XXXIth URSI, pp 1-4, Beijing, China, Aug. 16th-23rd (2014) (**Invited in special session**)

[30] Sule N., Hagness S. C., and Knezevic I., "Effects of charged impurity clusters on the conductivity of supported graphene," 20th International Conference on Electronic Properties of Two-Dimensional Systems (EP2DS-20), Wroclaw, Poland, July 1st-5th (2013).

[31] Sule N., Willis K. J., Hagness S. C., and Knezevic I., "Effects of charged impurity clusters on the conductivity of supported graphene," 16th International workshop on computational electronics (IWCE), Nara, Japan, June 4th-7th (2013). (**Outstanding Student Award**)

[32] Sule N., Willis K. J., Hagness S. C., and Knezevic I., "Numerical simulation of ac transport in graphene on an SiO2 substrate," The International Conference on Simulation of Semiconductor Pro- cesses and Devices (SISPAD), Denver CO, Sept. 5th-7th (2012).

[33] Sule N., Willis K. J., Hagness S. C., and Knezevic I., "Simulation of carrier dynamics in graphene on a substrate at terahertz and mid-infrared frequencies," 12th International Conference on Numerical Simulation of Optoelectronic Devices (NUSOD), Shanghai China, Aug. 28th-31st (2012).

[34] Sule N., Willis K. J., Hagness S. C., and Knezevic I., "Simulation of high-frequency carrier dynamics in graphene," 2012 IEEE International symposium on antennas and propagation and USNC-URSI national radio science meeting (AP-S/USNC-URSI), Chicago IL, July 8th-14th (2012). (**Invited in special session**)

[35] Sule N., Willis K. J., Hagness S. C., and Knezevic I., "Simulation of high-frequency carrier dynamics in graphene", 15th International workshop on computational electronics (IWCE), Madison WI, May 22nd-25th (2012). (**Honorable Mention for Outstanding Student Award**)

A list of *key* personnel involved in or supported by this research grant

Professors John Booske (Electrical and Computer Engineering), Irena Knezevic (Electrical and Computer Engineering), Susan Hagness (Electrical and Computer Engineering), Profesor Dane Morgan (Materials Science and Engineering),

Matt Kirley, Nishant Sule, and Ryan Jacobs (graduate students)